Chem

CellPress

Article

Graphite-Encapsulated Li-Metal Hybrid Anodes for High-Capacity Li Batteries

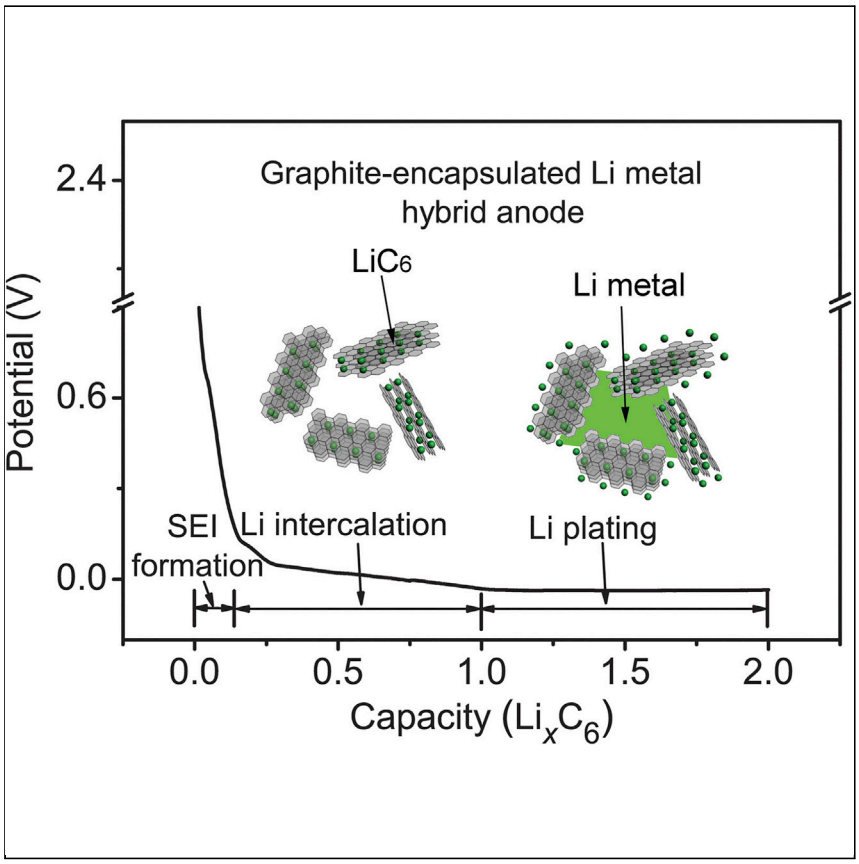

Graphite has long been the most used commercial anode material in Li-ion batteries. However, it has a limited Li intercalation capacity of 372 mAh g^{-1}, which cannot meet the increasing energy demand for Li-ion batteries. Here, we propose massive artificial graphite as a host material for the controlled deposition and stripping of Li metal within the internal space of the particles and demonstrate the surprisingly good electrochemical performance of such hybrid graphite-Li-metal anodes.

Yongming Sun, Guangyuan Zheng, Zhi Wei Seh, ..., Jie Sun, Hye Ryoung Lee, Yi Cui

yicui@stanford.edu

HIGHLIGHTS

A method for overcoming the capacity limit of graphite anode is provided

Li metal can be plated and stripped within massive artificial graphite particles

High Coulombic efficiency is achieved for the graphite-Li-metal hybrid anode

Sun et al., Chem 1, 287–297
August 11, 2016
http://dx.doi.org/10.1016/j.chempr.2016.07.009

Chem

CellPress

Article

Graphite-Encapsulated Li-Metal Hybrid Anodes for High-Capacity Li Batteries

Yongming Sun,[1] Guangyuan Zheng,[1] Zhi Wei Seh,[1] Nian Liu,[1] Shuang Wang,[2] Jie Sun,[1] Hye Ryoung Lee,[1] and Yi Cui[1,3,4,*]

SUMMARY

The drive to achieve high-energy-density lithium (Li)-ion batteries has attracted a tremendous amount of effort in the design of new materials. Although new electrode materials may take years, if not decades, to mature before they can become compatible with other components of Li-ion battery technology, exploring new phenomena on the existing electrode materials could offer many practical avenues for improving the existing technology. In this study, we report a convenient method of overcoming the capacity limit of conventional graphite anodes by reversibly plating and stripping Li metal within the internal space of massive artificial graphite particles. With a controlled specific capacity (744 mAh g^{-1}) twice that of the state-of-art for graphite, we obtained stable charge-discharge cycling with a high Coulombic efficiency of ~98.4% over more than 50 cycles at 0.2 C (74.4 mA g^{-1}) in a carbonate electrolyte.

INTRODUCTION

Graphite has long been the most used commercial anode material in lithium (Li)-ion batteries as a result of its high stability and low cost. However, because of a limited Li intercalation capacity (LiC_6, 372 mAh g^{-1}), it cannot meet the steadily increasing energy demand in many emerging applications, such as electric vehicles.[1] In the past 10 years, a lot of effort has gone into the development of alternative high-capacity anode materials beyond graphite, such as Si[2] and recently re-emerging Li metal.[3]

With the highest specific capacity (3,860 mAh g^{-1}) and lowest potential, Li metal is the holy grail of rechargeable batteries and was first studied nearly half a century ago.[4–9] In the mid-1970s, the Li battery was first developed by Exxon using bare Li metal as the anode and TiS_2 as the cathode.[4] An Li-MoS_2-type battery was manufactured by E-One Moli Energy as the first commercially available rechargeable Li power source.[10,11] However, as a result of its "hostless" nature during electroplating and stripping and a poorly controlled Li-electrolyte interface, Li metal has the disadvantage of the continuous formation of a highly resistive solid electrolyte interphase (SEI) and the growth of Li dendrites, and hence has inferior electrochemical performance and safety issues.[12–14] In the past decade, a great deal of research has been carried out to understand and control the process of Li-metal plating and stripping.[15–20] Various strategies, including exploring new electrolytes and electrolyte additives,[21–30] polymer and ceramic solid electrolytes,[31–33] nanoscale interfacial engineering on electrodes,[34–37] and three-dimensional (3D) current collectors,[38–42] have been successfully applied, but all the problems with building a viable Li-metal anode for practical application have not yet been solved.

The Bigger Picture

Lithium (Li)-ion battery technology has touched almost every aspect of our daily lives. Exploring new phenomena on existing electrode materials could offer many practical avenues for achieving high-energy-density Li-ion batteries. Graphite, the most commonly used commercial anode material, has a limited Li intercalation capacity (372 mAh g^{-1}). In this work, we show that massive artificial graphite electrodes with internal space within the particles allow stable Li-metal plating and stripping without the formation of Li dendrites. This entrapment of Li metal within the particles, together with the lithiation of graphite, allows the commercial anode to have a much higher specific capacity while maintaining a high Coulombic efficiency. Thus, the hybrid Li-storage mechanism of intercalation and plating, combined with a rational structure design for graphite, could be a promising strategy for tackling the intrinsic problem of low specific capacity in current commercial anodes.

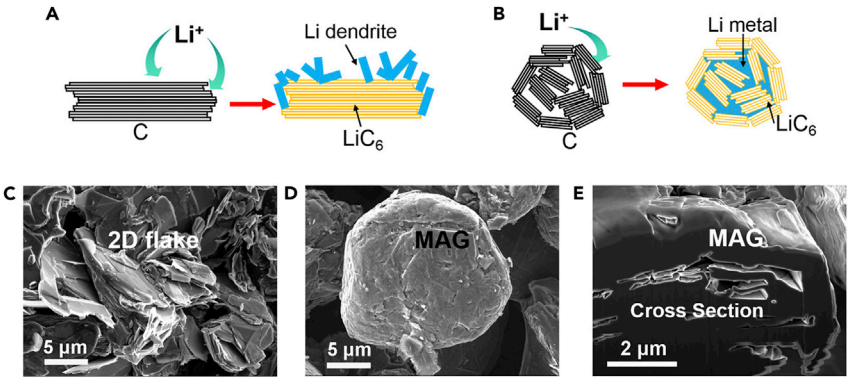

Figure 1. Illustration of Different Types of Graphite with Li-Metal Deposition

(A–D) Schematic illustration of (A) 2D graphite flakes and (B) MAG particles before and after Li-metal deposition and SEM images of (C) 2D graphite flakes and (D) MAG particles.

(E) A cross-sectional SEM image showing the internal pore space in the MAG particle.

Here, we propose graphite as a host material for the controlled deposition of Li metal and demonstrate the surprisingly good electrochemical performance of such hybrid graphite-Li-metal anodes. Graphite is a known material and would have a positive impact on battery applications if we are successful. However, there have been no clear studies on how Li metal deposits on graphite and the electrochemical dependence of Li deposition on different types of graphite. Although it is common knowledge that plating Li metal onto graphite during overcharge, fast, or low-temperature charging of batteries is a major safety issue, we believe that re-examining how Li metal is plated onto graphite could offer the opportunity of making graphite anodes safer and enabling Li-metal anodes.

The following features can make the concept of a graphite-Li-metal hybrid anode attractive and have a reasonable scientific basis. (1) During battery charging, Li ions would intercalate between graphene planes up to 372 mAh g^{-1} at a potential of 0.01–0.3 V versus Li. Beyond this capacity, Li metal starts to plate outside of graphite. It is well known that the edge planes of graphite are much more electrochemically active than the basal planes.[43–45] It was discovered that Li metal plates preferentially from the edge of graphite (see Figure S1). (2) Over the past decades, research on Li-ion batteries has created a number of morphologies for graphite, for example, natural graphite in the form of large two-dimensional (2D) flakes (Figure 1A, schematic drawing) and synthetic graphite in the form of massive artificial graphite (MAG), which consists of 3D packing of small 2D graphite flakes into a secondary particle (Figure 1B, schematic drawing). As shown in a scanning electron microscopy (SEM) image (Figure 1C), the 2D graphite flakes we investigated showed wide x-y dimensions (2–50 μm) parallel to the basal planes and a small z dimension perpendicular to the basal planes. Secondary micrometer-sized particles consisting of 3D packing of small 2D graphite flakes were observed for the MAG particles (Figure 1D; see also Figure S2). The small 2D graphite flakes within the MAG particles were packed with enormous quantities of edge planes (*c* dimension) (see Figure S2). The existence of internal pore space among the small 2D graphite flakes was confirmed by a cross-sectional SEM image of a MAG particle (Figure 1E). When Li metal was electroplated onto the 2D graphite flakes, it nucleated at the edge planes and grew outward toward organic electrolyte to directly form filaments and dendrites (Figure 1A, schematic drawing). However, it would be different for MAG because the surface of MAG particles is mainly in the basal plane, and the interior structure has many edge planes and some empty space. Li-metal deposition would

[1]Department of Materials Science and Engineering

[2]Department of Electrical Engineering Stanford University, Stanford, CA 94305, USA

[3]Stanford Institute for Materials and Energy Sciences, SLAC National Accelerator Laboratory, 2575 Sand Hill Road, Menlo Park, CA 94025, USA

[4]Lead Contact

*Correspondence: yicui@stanford.edu

http://dx.doi.org/10.1016/j.chempr.2016.07.009

preferably take place inside individual MAG particles, reducing direct contact with organic electrolyte (Figure 1B, schematic drawing). This would reduce the chance of Li-metal dendrite formation as well as the side chemical reaction with electrolyte. If we control the Li-metal capacity, it may be possible to fit all the deposited Li metal into the empty space inside individual MAG particles without growing out.

RESULTS

Characterizations of MAG Electrodes upon Li-Metal Deposition

The behavior of electrochemical Li-metal deposition for MAG particles and 2D graphite flakes was characterized in detail. Figures 2A–2C show the SEM images of the MAG and 2D graphite-flake electrodes after galvanostatic Li deposition with twice the specific capacity of conventional intercalation for a graphite anode (744 mAh g^{-1}), as well as a copper foil with the same amount of Li-metal deposition. The cross-sectional SEM image of a MAG electrode shows that the graphite particles closely stack on the copper foil (see Figure S3A). Although a rougher surface was observed after Li deposition as a result of the formation of SEI, there were no significant morphological changes before or after Li deposition (Figure 2A; see also Figures S3A and S3B), suggesting that Li plating happens inside the internal space of the MAG particles without the formation of Li dendrites on the surface of or inside the electrodes. We found a pronounced difference between the morphology of 2D graphite-flake electrodes after Li deposition and that of the MAG electrodes. Li dendrites formed easily on the surface of 2D graphite electrodes with large 2D graphite flakes without internal Li-storage space (Figure 2B). As controlled samples, Li deposition on copper-foil and carbon-black electrodes was also carried out. A large number of Li dendrites were clearly observed on the surface of the copper-foil and carbon-black electrodes (Figure 2C; see also Figures S3C and S3D).

Figure 2D shows the potential-composition trace of the initial electrochemical reaction process for the MAG and 2D graphite-flake electrodes at a constant current density of 0.1 C (37.2 mA g^{-1}) and a controlled specific capacity of 1,116 mAh g^{-1}. Overall, their charge and discharge curves are very similar. Their entire potential profiles exhibit several specific features, which can be divided into three different sections during the initial Li-deposition process: SEI formation, Li intercalation, and plating. A high overpotential is observed for the 2D graphite-flake electrodes at the beginning of Li plating (inset of Figure 2D), which may relate to the nucleation of Li dendrites. An ex situ X-ray diffraction (XRD) analysis was carried out to illustrate the Li-storage mechanism and the structural evolution of the MAG particle after galvanostatic Li intercalation and plating (Figures 2D–2F). XRD patterns were recorded for the samples at various stages. The corresponding cutoff capacity is indicated in the potential curve by markers (Figure 2D). Upon the charge process, a short sloping plateau at ~0.7 V was observed first and associated with the irreversible reactions with the electrolyte and formation of SEI. Pioneering research has been conducted on the physical chemistry and mechanism of intercalation in graphite.[46–48] There are several potential plateaus between 0.7 and 0.01 V, which can be attributed to the intercalation of Li between the graphene layers. To provide more insights on Li intercalation into MAG particles, the galvanostatic charge-discharge cycles for the MAG electrodes were measured at a low current density of 0.1 C using Li metal as both the counter and reference electrodes. As shown in Figure S3E, MAG typically showed three distinct potential plateaus (0.20, 0.11, and 0.07 V) for Li intercalation on its charge curves between 0.20 and 0.01 V. These plateaus correspond to two-phase coexistence regions caused by the stage transformations between dilute stages 1 and 4, stages 3 and 2, and stages 2 and 1 of Li-graphite intercalation compounds.[48–50] A reasonable capacity of 370 mAh g^{-1} (95–465 mAh g^{-1} in Figure S1,

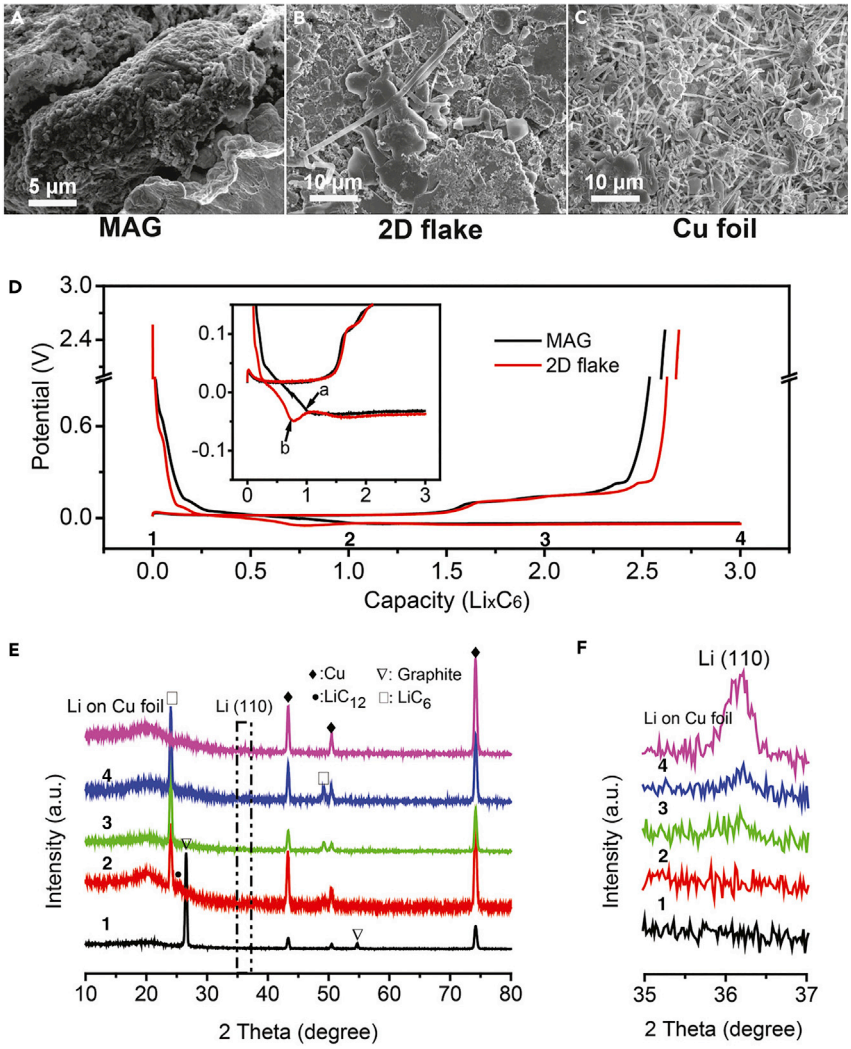

Figure 2. Characterizations of MAG and 2D Flake Electrodes upon Li-Metal Deposition

(A–C) SEM images of (A) MAG, (B) a 2D graphite-flake, and (C) copper-foil electrodes after Li-metal deposition with twice the capacity of conventional intercalation for a graphite anode.

(D) Electrochemical Li deposition for MAG particles and 2D flakes.

(E and F) XRD patterns of MAG and copper-foil electrodes after Li deposition at various stages. The dot-dash area in (E) shows the position of the strongest peak (110) of Li metal, which is magnified in (F). After Li deposition with three times the specific capacity of conventional intercalation, the MAG electrode exhibited a very weak and broad peak of Li metal. A much stronger and sharper peak for Li metal was observed for the copper foil after plating the same amount of Li.

corresponding to LiC_6) was obtained for MAG at 0.1 C during Li intercalation into the MAG particles. When a cell was further charged beyond LiC_6 stoichiometry (372 mAh g^{-1}) to Li_2C_6 (LiC_6 + Li: 744 mAh g^{-1}) and Li_3C_6 (LiC_6 + 2Li: 1,116 mAh g^{-1}), a long potential plateau at ~−0.01 V was observed as a result of the plating of Li metal in the graphite electrode. Adjusting the plating time could control the total content of deposited Li. Figures 2E and 2F show the ex situ XRD spectra of the electrodes corresponding to the four stages with different amounts of Li intercalation and plating (x in Li_xC_6): (1) C, (2) LiC_6, (3) Li_2C_6, and (4) Li_3C_6. Significant broadening and reduced intensity were observed for the (110) peak of Li metal in (3) Li_2C_6 and (4) Li_3C_6, indicating the nanocrystalline nature. The appearance of the Li-metal signature confirms Li-metal plating as the primary reaction mechanism after intercalation of Li between the graphene layers. In

particular, confined by the small and isolated space within the MAG particles, large Li-metal crystallites do not grow. For comparison, there was a much stronger signature of Li metal after the same amount of Li was plated onto a copper foil because of a much larger crystallite size (Figures 2E and 2F). Moreover, the Li metal in (3) Li_2C_6 and (4) Li_3C_6 could be stripped, and the Li in (2) LiC_6, (3) Li_2C_6, and (4) Li_3C_6 could also be de-intercalated reversibly. All the product at various stages could be fully recharged back to graphite (see Figure S3F).

MAG Electrodes with Different Total Li-Metal Capacity and Current-Density Dependence

Investigations were carried out to examine how much Li metal can deposit on MAG electrodes and the relationship between different current densities and the formation of Li dendrites. The morphology of the MAG electrodes after galvanostatic Li deposition with a controlled capacity of 744, 930, and 1,116 mAh g^{-1} at 0.2 C (74.4 mA g^{-1}) are compared in Figures 3A–3C. We did not observe Li-metal growth with a controlled capacity of 744 mAh g^{-1} (twice the capacity of graphite intercalation, Figure 3A). To further investigate the pores within MAG particles before and after Li deposition, we performed dual-beam focused ion beam (FIB) analysis and cross-sectional SEM by using an FEI Helios 600i FIB/SEM system. A focused gallium-ion beam was used for vertical dissection at the desired locations of MAG particles and MAG electrodes before and after Li deposition. As a result of the melting and merging of the pores during the milling process, only big pores remained, as shown in the images. As observed from the cross-sectional SEM image of MAG particles (Figures 1E and S3G), the remaining pore volume was ~25%. After Li deposition, the pores were almost filled (Figure S3H). However, as Li continued to plate, Li dendrites grew out of the MAG electrode after the deposition of 2.5 times the intercalation capacity (930 mAh g^{-1} based on the mass of graphite, Figure 3B). Furthermore, with three times the capacity of graphite intercalation, islands of Li dendrites formed and interconnected with each other on the surface of the MAG electrode (Figure 3C), similar to the Li dendrites formed on the surface of a carbon-black electrode (see Figures S3C and S3D). SEM images of the MAG electrodes after Li-metal deposition at 0.4 and 0.6 C with a controlled capacity of 744 mAh g^{-1} were also examined (Figures 3D and 3E). When the current density increased to 0.4 C, a number of Li dendrites were observed on the surface of the MAG electrodes. Because of the limited rate capability of graphite, the growth of Li dendrites on the surface of the electrodes was facilitated when the charging current density increased. The growth of Li dendrites may decay battery performance during cycling and may cause safety issues. Li metal or dendrites with an open structure react with the electrolyte continuously during battery cycling. When Li-metal plating and stripping take place without a host material or outside a host material, the initially formed SEI cannot withstand mechanical deformation and continuously breaks and repairs during cycling. This leads to continuous consumption of electrolyte and thus low Coulombic efficiency over cycling and a limited cycle life of the Li-metal anode. In contrast, when Li metal is confined inside a host material, the electrolyte is blocked on the outside surface of the host material and does not come into contact with Li directly. SEI formation happens only on the outside surface of the host material. After the initial formation cycles, the SEI becomes stable and protects the electrolyte from further decomposition. Therefore, for the MAG electrodes used here, we limited the rate to 0.2 C and the capacity to 744 mAh g^{-1}.

Electrochemical Measurement of the MAG-Li-Hybrid Anode

The MAG, 2D graphite-flake, and copper-foil electrodes were cycled in a carbonate electrolyte using Li foil as the counter electrode. A fair comparison of their electrochemical performance was carried out with the same mass loading of electrode

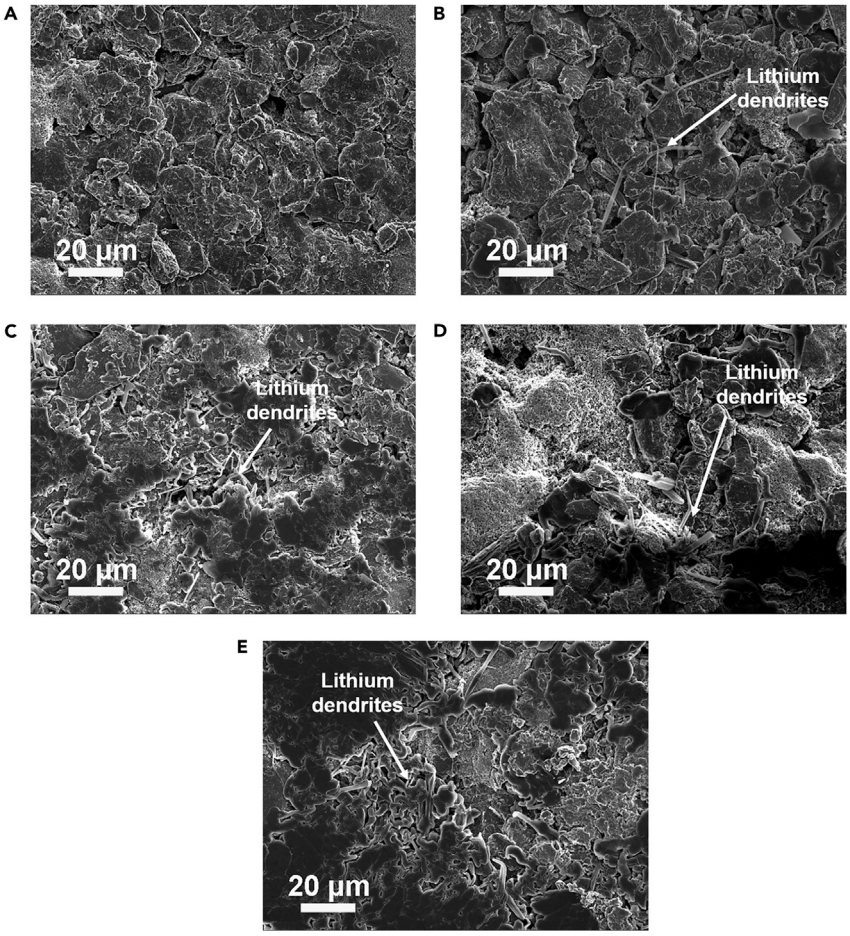

Figure 3. MAG Electrodes with Different Total Li-Metal Capacity and Current-Density Dependence

(A–C) SEM images of a MAG electrode after Li deposition at 0.2 C with (A) 2, (B) 2.5, and (C) 3 times the capacity of conventional intercalation. After deposition of 2.5 times the Li intercalation capacity, Li dendrites grew out of the MAG electrode. Islands of Li dendrites formed and tended to interconnect with each other on the surface of the MAG electrode with three times the capacity of graphite intercalation.

(D and E) SEM images of the MAG electrodes after Li deposition at (D) 0.4 and (E) 0.6 C with twice the capacity of conventional intercalation. When the current density increased to 0.4 C, Li dendrites were observed on the surface of MAG electrodes. Thus, at more than twice the Li intercalation capacity, the interior space of MAG was not enough to hold the Li metal, and the dendrites came out. On the other hand, even with enough interior space, Li dendrites grew out from the MAG when the current increased to 0.4 C. The growth of the Li dendrites was facilitated by increasing charging current densities. The current rate C was based on the intercalation specific capacity of graphite (372 mAh g^{-1}).

materials (MAG and 2D graphite flake) and the same amount of electrolytes, as well as the deposition of the same amount of Li for all the electrodes. Coulombic efficiency is vital for practical electrodes in rechargeable batteries and is calculated as the extraction versus the intercalation and plating capacity. As a result of the excess Li in the Li-metal counter electrode, the Coulombic efficiency can be used for evaluating the active loss of working electrodes. In a conventional graphite-Li-metal half-cell, Li can be electrochemically intercalated into the layer structure of graphite reversibly above 0 V. Thus, a stable Coulombic efficiency above 99% was obtained (see Figure S4A). Here, a controlled Li specific capacity of 744 mAh g^{-1} at 0.2 C, which is double the theoretical intercalation capacity of graphite, was

deposited onto the MAG electrode and 2D graphite-flake electrodes. Therefore, besides Li intercalation into the graphite interlayers (372 mAh g^{-1}), another half of Li deposited on the electrode in the form of Li metal. For the MAG electrode, Coulombic efficiency starts at 83.4%, quickly rises to 98.4%, and remains stable for more than 80 cycles, which is very close to the cycling obtained above 0 V (Figure 4A; see also Figure S4A). For comparison, the 2D graphite electrode exhibited a lower Coulombic efficiency upon cycling. Its Coulombic efficiency was 91.8% at the 50^{th} cycle, lower than the 97.5% for the MAG electrode, as a result of the formation of Li dendrites on the surface of the electrode. With regard to the effect of current when normalized to the actual area for Li deposition, the number of edge planes of graphite within MAG particles reduces the local current density, which may lead to uniform deposition of Li metal within the MAG particles and thus improve the Coulombic efficiency. To eliminate the effect of the loss of Li metal in MAG-Li-metal half cells, MAG-$LiCoO_2$ cells were assembled with $LiCoO_2$ electrodes as the counter electrodes and Li sources. Impressively, a high Coulombic efficiency of 98.8% was achieved even after 100 cycles (see Figure S4B). Although Li metal is known to have very low Coulombic efficiency in carbonate electrolytes, the high Coulombic efficiency with very low variation during cycling in MAG suggests the formation of a stable SEI and the reduction of electrolyte decomposition. In contrast, the copper-foil electrode showed a noticeable drop in Coulombic efficiency from 92.1% to 59.9% after 50 cycles. The low Coulombic efficiency and its fast degradation over cycling originate from the continuous reaction between Li dendrites and electrolyte due to unstable SEI. The rapid decay in Coulombic efficiency is in agreement with the continuously increasing surface area and irreversible reaction between electrolyte and Li dendrites, which is totally different from that of the graphite electrode.

To examine the electrochemical performance of the graphite electrodes, we deposited the same amount of Li metal as that of the copper foil electrode, corresponding to a very high specific capacity of 1,116 mAh g^{-1} for the MAG. Although some Li metal grew out from the electrodes (Figure 3C), the electrode still exhibited a high Coulombic efficiency of 96.6% at the tenth cycle and remained at 95.1% after 30 cycles (see Figure S4C), demonstrating significant improvement over the copper-foil electrode (Figure 4A). The great improvement in Coulombic efficiency over cycling indicates that the surface area of Li metal exposed to the electrolyte is significantly reduced and the irreversible reaction between the Li metal and electrolyte is significantly suppressed. The effect of the reduction in electrolyte decomposition and the formation of a stable SEI can be confirmed by the reduction of polarization in the voltage profile of a graphite electrode during cycling (Figure 4B). It was clearly observed that the voltage profiles over cycling coincided well at the potentials of Li intercalation and plating and extraction and stripping after the initial cycle. The voltage for Li plating was only ~−30 mV in the initial cycle (Figure 4C), whereas it was ~−70 mV for the copper-foil electrode (Figure 4D). The voltage for Li stripping was ~25 mV in the initial cycle (Figures 4C and 4D). The voltage hysteresis of the two electrodes over 50 cycles is shown in Figure 4E. For the MAG electrode, voltage hysteresis for Li plating and stripping remained stable and was only ~42 mV after 50 cycles. Compared with the voltage hysteresis of ~97 mV for the copper-foil electrode, that for the MAG electrode was much smaller, indicating the low internal resistance arising from the preservation of a stable and thin SEI layer on the surface of the MAG electrode.

DISCUSSION

In this work, we have shown that MAG electrodes with internal space within the particles allow stable Li-metal plating and stripping without the formation of Li

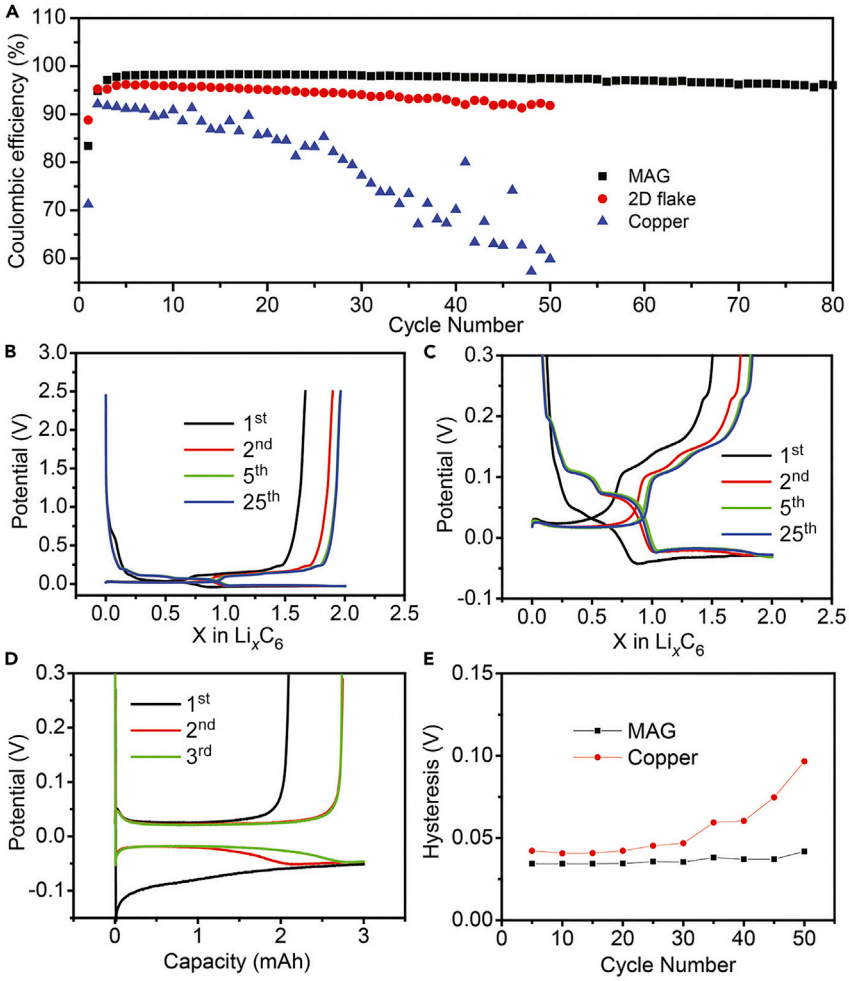

Figure 4. Electrochemical Performance of MAG-Li-Metal Hybrid Electrodes

(A) Coulombic efficiency of MAG, 2D graphite-flake and copper-foil electrodes over cycling with Li metal as the reference and counter electrode.

(B and C) Voltage profiles of a MAG electrode for the 1st, 2nd, 5th, and 25th cycles. The voltage profile in (B) is expanded in (C) to show −0.1 to 0.3 V.

(D) Voltage profiles for Li plating and stripping on a copper-foil electrode for the initial three cycles.

(E) Voltage hysteresis of MAG and copper-foil electrodes over cycling. The current density was 0.2 C on the basis of the intercalation specific capacity of graphite (74.4 mA g^{-1}).

dendrites. This entrapment of Li metal within the particles, together with the lithiation of graphite, allows a commercial anode to have a much higher specific capacity while maintaining high Coulombic efficiency. With a controlled capacity of 744 mAh g^{-1}, a MAG electrode exhibited excellent reversibility and high Coulombic efficiency of ~98.4% with stable cycling for 50 cycles. This is significantly better than plating and stripping of Li metal onto a copper-foil counterpart, which exhibits much larger voltage hysteresis and faster decay in Coulombic efficiency as a result of the unstable SEI and the growth of Li dendrites. Because of the instability of the SEI and the high reactivity of Li metal, Li-metal batteries have low Coulombic efficiency in both carbonate-based electrolytes (80%–90%) and ether-based electrolytes (90%–95%).[51] Although exciting progress has been achieved recently in research on Li-metal anodes, their Coulombic efficiency is still low for practical application, especially in reactive carbonate electrolyte, which is

the most widely used commercial electrolyte in the industry. The Coulombic efficiency achieved here is one of the best results for Li-metal anodes to date.[34,39,52] Another important point to be noted here is that commercial carbonate electrolyte was used directly in our battery testing. Therefore, our work may have great commercial value for making existing anodes work with much higher specific capacity far beyond the theoretical limit of traditional understanding. Overall, the idea of engineering a graphite structure for the entrapment of Li metal provides a promising strategy for solving the low-energy-density limit of the conventional graphite anode. Further increases in Coulombic efficiency (e.g., >99.5%) will be achieved in future work with better structure designs for graphite and electrolyte additives.

EXPERIMENTAL PROCEDURES

Materials and Characterization

MAG particles and 2D graphite flakes were used as received. Morphology characterization was carried out using FEI XL30 Sirion SEM with a field emission gun. For observing the electrodes after Li intercalation and plating, the working electrodes were rinsed in dimethyl carbonate after the coin cells were disassembled in an argon-filled glove box. These electrodes were sealed before being transferred into the SEM chamber. XRD patterns were obtained with a PANalytical X'Pert Diffractometer (Cu Kα radiation, λ = 1.5406 Å). The electrodes for XRD measurements were tightly sealed with Kapton tape in an inert atmosphere. The cross-sectional images of the MAG particles were acquired on an FEI Helios NanoLab 600i DualBeam FIB/SEM system, which combined SEM imaging and FIB milling. A focused gallium-ion beam was used for vertical dissection at the desired locations to expose the interior of a MAG particle.

Electrochemical Measurements

Graphite powder, Super P carbon black, and polyvinyldifluoride (PVDF) were mixed together in a weight ratio of 8:1:1 in *N*-methyl-pyrrolidone solvent. The slurries were coated onto a copper-foil current collector by a doctor-blading method and dried in a vacuum to form the working electrodes. A typical mass loading of the electrodes was ~2 mg/cm^2. The control carbon-black electrode was fabricated by the same procedure. The weight ratio of carbon black and PVDF in the electrodes was 7:3. A copper foil was used directly as another control electrode. Coin cells (CR2032, MTI Corporation) were assembled in an argon-filled glove box. A Celgard 2250 membrane was used as the separator, and a Li foil (Alfa Aesar) was used as the counter electrode and reference electrode. The electrolyte was a solution of 1 M $LiPF_6$ in 1:1 w/w ethylene carbonate/diethyl carbonate. The galvanostatic measurements were measured on a 96-channel battery tester (Arbin Instruments). Galvanostatic Li intercalation and plating were carried out at a desired capacity and current density (0.2 C based on graphite). The extraction and stripping of Li were performed at the same current rate with a cutoff voltage of 2.5 V. Coulombic efficiency was calculated on the basis of the capacity between intercalation and plating and extraction and stripping. The average voltage hysteresis was calculated on the basis of the average value of the corresponding Li plating and stripping plateaus.

SUPPLEMENTAL INFORMATION

Supplemental Information includes four figures and can be found with this article online at http://dx.doi.org/10.1016/j.chempr.2016.07.009.

AUTHOR CONTRIBUTIONS

Y.S., G.Z., Z.W.S., N.L., S.W., and Y.C. conceived the concept and experiments. Y.S., J.S., and H.R.L. performed material characterization and electrochemical measurements. Y.S. and Y.C. co-wrote the paper. All authors discussed the results and commented on the manuscript.

ACKNOWLEDGMENTS

Y.C. acknowledges support from the Assistant Secretary for Energy Efficiency and Renewable Energy in the Vehicle Technologies Office of the U.S. Department of Energy. G.Z. and Z.W.S. acknowledge financial support from the Agency for Science, Technology, and Research (A*STAR) in Singapore.

Received: April 25, 2016
Revised: July 7, 2016
Accepted: July 20, 2016
Published: August 11, 2016

REFERENCES AND NOTES

1. Dahn, J.R., Zheng, T., Liu, Y.H., and Xue, J.S. (1995). Mechanisms for lithium insertion in carbonaceous materials. Science *270*, 590–593.
2. Chan, C.K., Peng, H.L., Liu, G., Mcilwrath, K., Zhang, X.F., Huggins, R.A., and Cui, Y. (2008). High-performance lithium battery anodes using silicon nanowires. Nat. Nanotech. *3*, 31–35.
3. Zheng, G.Y., Lee, S.W., Liang, Z., Lee, H.-W., Yan, K., Yao, H.B., Wang, H.T., Li, W.Y., Chu, S., and Cui, Y. (2014). Interconnected hollow carbon nanospheres for stable lithium metal anodes. Nat. Nanotech. *9*, 618–623.
4. Whittingham, M.S. (1976). Electrical energy storage and intercalation chemistry. Science *192*, 1126–1127.
5. Whittingham, M.S. (February 1977). Chalcogenide Battery. US patent 4009052.
6. Tarascon, J.-M., and Armand, M. (2001). Issues and challenges facing rechargeable lithium batteries. Nature *414*, 359–367.
7. Bruce, P.G., Freunberger, S.A., Hardwick, L.J., and Tarascon, J.-M. (2012). Li-O2 and Li-S batteries with high energy storage. Nat. Mater. *11*, 19–29.
8. Xu, W., Wang, J.L., Ding, F., Chen, X.L., Nasybulin, E., Zhang, Y.H., and Zhang, J.G. (2014). Lithium metal anodes for rechargeable batteries. Energy Environ. Sci. *7*, 513–537.
9. Kim, H., Jeong, G., Kim, Y.-U., Kim, J.-H., Park, C.-M., and Sohn, H.-J. (2013). Metallic anodes for next generation secondary batteries. Chem. Soc. Rev. *42*, 9011–9034.
10. Laman, F.C., Matsen, M.W., and Stiles, J.A.R. (1986). Inductive impedance of a spirally wound Li/MoS2 cell. J. Electrochem. Soc. *133*, 2441–2446.
11. Stiles, J.A.R. (1985). New mater. New Process *3*, 89.
12. Scrosati, B., and Garche, J. (2010). Lithium batteries: status, prospects and future. J. Power Sources *195*, 2419–2430.
13. Lv, D.P., Shao, Y.Y., Lozano, T., Bennett, W.D., Graff, G.L., Polzin, B., Zhang, J.G., Engelhard, M.H., Saenz, N.T., Henderson, W.A., et al. (2014). Failure mechanism for fast-charged lithium metal batteries with liquid electrolytes. Adv. Energy Mater. *5*, 1400993.
14. Armand, M., and Tarascon, J.-M. (2008). Building better batteries. Nature *451*, 652–657.
15. Harry, K.J., Hallinan, D.T., Parkinson, D.Y., MacDowell, A.A., and Balsara, N.P. (2014). Detection of subsurface structures underneath dendrites formed on cycled lithium metal electrodes. Nat. Mater. *13*, 69–73.
16. Chandrashekar, S., Trease, N.M., Chang, H.J., Du, L.-S., Grey, C.P., and Jerschow, A. (2012). 7Li MRI of Li batteries reveals location of microstructural lithium. Nat. Mater. *11*, 311–315.
17. Bhattacharyya, R., Key, B., Chen, H.L., Best, A.S., Hollenkamp, A.F., and Grey, C.P. (2010). In situ NMR observation of the formation of metallic lithium microstructures in lithium batteries. Nat. Mater. *9*, 504–510.
18. Gireaud, L., Grugeon, S., Laruelle, S., Yrieix, B., and Tarascon, J.-M. (2006). Lithium metal stripping/plating mechanisms studies: a metallurgical approach. Electrochem. Commun. *8*, 1639–1649.
19. Aurbach, D., and Cohen, Y. (1996). The application of atomic force microscopy for the study of Li deposition processes. J. Electrochem. Soc. *143*, 3525–3532.
20. Orsini, F., Pasquier, A.D., Beaudoin, B., Tarascon, J.-M., Trentin, M., Langenhuizen, N., Beer, E.D., and Notten, P. (1998). In situ scanning electron microscopy (SEM) observation of interfaces within plastic lithium batteries. J. Power Sources *76*, 19–29.
21. Hirai, T., Yoshimatsu, I., and Yamaki, J.-I. (1994). Effect of additives on lithium cycling efficiency. J. Electrochem. Soc. *141*, 2300–2305.
22. Ding, F., Xu, W., Graff, G.L., Zhang, J., Sushko, M.L., Chen, X.L., Shao, Y.Y., Engelhard, M.H., Nie, Z.M., Xiao, J., et al. (2013). Dendrite-free lithium deposition via self-healing electrostatic shield mechanism. J. Am. Chem. Soc. *135*, 4450–4456.
23. Lee, Y.M., Seo, J.E., Lee, Y.-G., Lee, S.H., Cho, K.Y., and Park, J.-K. (2007). Effects of triacetoxyvinylsilane as SEI layer additive on electrochemical performance of lithium metal secondary battery. Electrochem. Solid State Lett. *10*, A216–A219.
24. Shiraishi, S., Kanamura, K., and Takehara, Z.-I. (1999). Surface condition changes in lithium metal deposited in nonaqueous electrolyte containing HF by dissolution-deposition cycles. J. Electrochem. Soc. *146*, 1633–1639.
25. Crowther, O., and West, A.C. (2008). Effect of electrolyte composition on lithium dendrite growth. J. Electrochem. Soc. *155*, A806–A811.
26. Ota, H., Shima, K., Ue, M., and Yamaki, J.-i (2004). Effect of vinylene carbonate as additive to electrolyte for lithium metal anode. Electrochim. Acta *49*, 565–572.
27. Miao, R.R., Yang, J., Feng, X.J., Jia, H., Wang, J.L., and Nuli, Y. (2014). Novel dual-salts electrolyte solution for dendrite-free lithium-metal based rechargeable batteries with high cycle reversibility. J. Power Sources *271*, 291–297.
28. Zhang, Y.H., Qian, J.F., Xu, W., Russell, S.M., Chen, X.L., Nasybulin, E., Bhattacharya, P., Engelhard, M.H., Mei, D.H., Cao, R.G., et al. (2014). Dendrite-free lithium deposition with self-aligned nanorod structure. Nano Lett. *14*, 6889–6896.
29. Qian, J.F., Henderson, W.A., Xu, W., Bhattacharya, P., Engelhard, M., Borodin, O., and Zhang, J.-G. (2015). High rate and stable cycling of lithium metal anode. Nat. Commun. *6*, 6362.
30. Li, W.Y., Yao, H.B., Yan, K., Zheng, G.Y., Liang, Z., Chiang, Y.-M., and Cui, Y. (2015). The synergetic effect of lithium polysulfide and lithium nitrate to prevent lithium dendrite growth. Nat. Commun. *6*, 7436.

31. Croce, F., Appetecchi, G.B., Persi, L., and Scrosati, B. (1998). Nanocomposite polymer electrolytes for lithium batteries. Nature *394*, 456–458.

32. Kamaya, N., Homma, K., Yamakawa, Y., Hirayama, M., Kanno, R., Yonemura, M., Kamiyama, T., Kato, Y., Hama, S., Kawamoto, K., and Mitsui, A. (2011). A lithium superionic conductor. Nat. Mater. *10*, 682–686.

33. Bouchet, R., Maria, S., Meziane, R., Aboulaich, A., Lienafa, L., Bonnet, J.-P., Phan, T.N.T., Bertin, D., Gigmes, D., Devaux, D., et al. (2013). Single-ion BAB triblock copolymers as highly efficient electrolytes for lithium-metal batteries. Nat. Mater. *12*, 452–457.

34. Yan, K., Lee, H.-W., Gao, T., Zheng, G.Y., Yao, H.B., Wang, H.T., Lu, Z.D., Zhou, Y., Liang, Z., Liu, Z.F., et al. (2014). Ultrathin two-dimensional atomic crystals as stable interfacial layer for improvement of lithium metal anode. Nano Lett. *14*, 6016–6022.

35. Liang, Z., Zheng, G.Y., Liu, C., Liu, N., Li, W.Y., Yan, K., Yao, H.B., Hsu, P.-C., Chu, S., and Cui, Y. (2015). Polymer nanofiber-guided uniform lithium deposition for battery electrodes. Nano Lett. *15*, 12910–12916.

36. Kozen, A.C., Lin, C.-F., Pearse, A.J., Schroeder, M.A., Han, X.G., Hu, L.B., Lee, S.-B., Rubloff, G.W., and Noked, M. (2015). Next-generation lithium metal anode engineering via atomic layer deposition. ACS Nano *9*, 5884–5892.

37. Li, N.-W., Yin, Y.-X., Yang, C.-P., and Guo, Y.-G. (2015). An artificial solid electrolyte interphase layer for stable lithium metal anodes. Adv. Mater. *9*, 1853–1858.

38. Zhang, R., Cheng, X.-B., Zhao, C.-Z., Peng, H.-J., Shi, J.-L., Huang, J.-Q., Wang, J.F., Wei, F., and Zhang, Q. (2016). Conductive nanostructured scaffolds render low local current density to inhibit lithium dendrite growth. Adv. Mater. *28*, 2155–2162.

39. Liang, Z., Lin, D., Zhao, J., Lu, Z., Liu, Y., Liu, C., Lu, Y., Wang, H., Yan, K., Tao, X., and Cui, Y. (2016). Composite lithium metal anode by melt infusion of lithium into a 3D conducting scaffold with lithiophilic coating. Proc. Natl. Acad. Sci. USA *113*, 2862–2867.

40. Liu, Y., Lin, D., Liang, Z., Zhao, J., Yan, K., and Cui, Y. (2016). Lithium-coated polymetric matrix as a minimum-volume-change and dendrite-free lithium metal anode. Nat. Commun. *7*, 10992.

41. Lin, D., Liu, Y., Liang, Z., Lee, H.-W., Sun, J., Wang, H., Yan, K., Xie, J., and Cui, Y. (2016). Layered reduced graphene oxide with nanoscale interlayer gaps as a stable host for lithium metal anode. Nat. Nanotech. *11*, 626–632.

42. Ji, X., Liu, D.-Y., Prendiville, D.G., Zhang, Y., Liu, X., and Stucky, G.D. (2012). Spatially heterogeneous carbon-fiber papers as surface dendrite-free current collectors for lithium deposition. Nano Today *7*, 10–20.

43. Karim, Z., Gabrielle, N., and Kimio, K. (2000). Effect of graphite particle size on irreversible capacity loss. J. Electrochem. Soc. *147*, 2110–2115.

44. Banks, C.E., Davies, T.J., Wildgoose, G.G., and Compton, R.G. (2005). Electrocatalysis at graphite and carbon nanotube modified electrodes: edge-plane sites and tube ends are the reactive sites. Chem. Commun. 829–841.

45. Shen, A., Zou, Y., Wang, Q., Dryfe, R.A.W., Huang, X., Dou, S., Dai, L., and Wang, S. (2014). Oxygen reduction reaction in a droplet on graphite: direct evidence that the edge is more active than the basal plane. Angew. Chem. *126*, 10980–10984.

46. Hooley, J.G. (1977). Physical chemistry and mechanism of intercalation in graphite. Mater. Sci. Eng. *31*, 17–24.

47. Hooley, J.G. (1992). The effect of flake thickness on the intercalation of graphite. Carbon *10*, 155–163.

48. Funabiki, A., Inaba, M., Abe, T., and Ogumi, Z. (1999). Stage transformation of lithium-graphite intercalation compounds caused by electrochemical lithium intercalation. J. Electrochem. Soc. *146*, 2443–2448.

49. Levi, M.D., and Aurbach, D. (1997). The mechanism of lithium intercalation in graphite film electrodes in aprotic media. Part 1. High resolution slow scan rate cyclic voltammetric studies and modeling. J. Electroanal. Chem. *421*, 79–88.

50. Dahn, J.R. (1991). Phase diagram of LixC6. Phys. Rev. B *44*, 9170–9177.

51. Ota, H., Sakata, Y., Wang, X., Sasahara, J., and Yasukawa, E. (2004). Characterization of lithium electrode in lithium imides/ethylene carbonate, and cyclic ether electrolytes: I. Surface morphology and lithium cycling efficiency. J. Electrochem. Soc. *151*, A427–A436.

52. Luo, W., Zhou, L., Fu, K., Yang, Z., Wan, J., Manno, M., Yao, Y., Zhu, H., Yang, B., and Hu, L. (2015). A thermally conductive separator for stable Li metal anodes. Nano Lett. *15*, 6149–6154.